

**Density functional theory plus dynamical mean-field theory with natural atomic orbital projectors**Jae-Hoon Sim and Myung Joon Han <sup>\*</sup>*Department of Physics, Korea Advanced Institute of Science and Technology (KAIST), Daejeon 34141, Korea*

(Received 23 May 2019; published 25 September 2019)

We introduce natural atomic orbitals as the local projector to define the correlated subspace for DFT + DMFT (density functional theory plus dynamical mean-field theory) calculation. The natural atomic orbitals are found to be stably constructed against the number and the radius of basis orbitals. It can also be self-consistently updated inside the DFT+DMFT loop. The spatial localization, electron occupation and the degree of correlation are investigated and compared with other conventional techniques. As a “natural” choice to describe the electron numbers, adopting natural atomic orbitals has advantage in terms of electron number counting. We further explore the reduction of computation cost by separating correlated orbitals into two subgroups based on the orbital occupancy. Our new recipe can serve as a useful choice for DFT+DMFT and related methods.

DOI: [10.1103/PhysRevB.100.115151](https://doi.org/10.1103/PhysRevB.100.115151)**I. INTRODUCTION**

The calculation of real materials with strong electronic correlations poses an important problem in condensed matter physics and material science. While the first-principles band structure method based on density functional theory (DFT) provides a powerful theoretical framework for real materials, the sizable on-site correlation invalidates the standard approximations such as local density approximation (LDA) and generalized gradient approximation (GGA). To overcome this limitation, the combined methods of LDA/GGA with many-body techniques have been suggested and made tremendous success such as the early attempts of so-called LDA+ $U$  or DFT+ $U$  [1,2] and the more recently suggested LDA+Gutzwiller [3–6].  $GW$  type of self energy within the self-consistent framework [7–9] can also be useful with the limited purposes of, e.g., describing the model parameters and the metallic Fermi surfaces [10,11]. Among them, DFT+DMFT (dynamical mean-field theory) has become one of the standard choices providing the unique feature by capturing the “dynamic” correlations [12–18].

Along with its great success, many of formal and technical issues in the implementation have received much attention [19–31]. Typically, any attempt to combine LDA/GGA-type of scheme with Hubbard-like model approach requires a step to define the correlated subspace within which Coulomb interaction (“Hubbard  $U$ ”) comes in to play. In other words, the correlated orbitals span the bands near the Fermi level ( $E_F$ ) where the on-site correlation becomes important. They are expected to be reasonably well localized, site-centered and atomic-like. In literature, many different suggestions to define the correlated orbital space are found: maximally localized Wannier functions (MLWF) [32,33], muffin-tin orbitals [34,35], and other projection methods [31,36].

Considering the ambiguity in this choice of “projector,” we take a special note of recent studies that emphasize the correlated orbital occupancy  $N_d$  being the critical variable to describe the correlation effect [37,38]. Here it should first be noted that estimating or determining  $N_d$  is a nontrivial issue. It depends on the form of so-called double counting form [37,38] as well as the choice of the correlated orbitals [36]. In fact, it is not straightforward already in DFT-LDA level, leading to many different possible choices suggested for atomic orbitals or charge counting schemes such as Mulliken population analysis [39,40], Löwdin orthogonalization method [41], and natural population analysis [42].

In this paper, we suggest the implementation of DFT+DMFT with natural atomic orbitals (NAOs) as the local projector. In our DFT formulation based on the linear combination of nonorthogonal pseudo-atomic orbitals (PAOs) [43], the use of NAOs provides a ‘natural’ way of estimating  $N_d$  from the orthogonalized orbitals. The NAO construction process is not only well plugged in between DFT and DMFT self-consistent loop, but it also stable with respect to the numerical parameters such as the range of energy window and the number of basis sets. Our calculations show that the localization and the covalency are reasonably well described with NAO compared with the other choices including PAO, Löwdin orthogonalized orbital (LOO), and MLWF. Further, the possibility of reducing computation cost is explored by separating the correlated subspace into two different parts.

The paper is organized as follow. In Sec. II, we briefly review the DFT+DMFT procedure which is followed by our NAO-based formalism. In Sec. III, the calculation results are presented for a correlated metal SrVO<sub>3</sub> and a charge-transfer insulator NiO. Summary and conclusion are given in Sec. IV.

**II. FORMALISM****A. DFT+DMFT and the basis issue**

So-called DFT+DMFT is a scheme that combines the standard band theory such as LDA and GGA with a nonperturbative many-body technique, DMFT. In DMFT, the lattice

<sup>\*</sup>mj.han@kaist.ac.kr

self-energy  $\hat{\Sigma}_{\text{latt}}(i\omega_n, \mathbf{k})$  is approximated by local self-energy  $\hat{\Sigma}_{\text{latt}}^{\text{DMFT}}(i\omega_n) = \bigoplus_R \hat{\Sigma}_{\text{loc}}(R)$ . The nonlocal contribution is projected out by a local projection;  $\hat{\Sigma}_{\text{loc}}(R) = P_R \hat{\Sigma}_{\text{latt}} = \sum_{\alpha\beta \in d} |\chi_{\alpha R}\rangle \Sigma_{\alpha\beta}(R) \langle \chi_{\beta R}|$ , where “ $d$ ” refers to the correlated subspace such as transition-metal  $d$  orbitals and  $R$  the atomic position. The on-site Coulomb interaction is applied onto the localized orbitals  $|\chi_{\alpha}\rangle$ . The interacting Green’s function is given by

$$\hat{G}(i\omega_n, \mathbf{k}) = \frac{1}{i\omega_n + \mu - \hat{H}(\mathbf{k}) - \hat{\Sigma}_{\text{loc}}(i\omega_n) + \hat{\Sigma}_{\text{dc}}(i\omega_n)}, \quad (1)$$

where  $\hat{\Sigma}_{\text{dc}}$  refers to the double-counting term. Once  $P_R$ , or correlated subspace  $\{|\chi_{\alpha}\rangle\}$  is specified,  $\hat{\Sigma}_{\text{loc}}$  is determined by solving the impurity model with the self-consistently-constructed hybridization function [12–14,16]:

$$\hat{\Delta}(i\omega_n) = P_{R=0} \left[ i\omega_n - \hat{H}_{\text{loc}} - \Sigma_{\text{loc}}(i\omega_n) + \Sigma_{\text{dc}}(i\omega_n) - \left( \frac{1}{N_k} \sum_k \hat{G}(\mathbf{k}, i\omega_n) \right)^{-1} \right]. \quad (2)$$

Many issues can arise in solving this problem. The first thing is to choose “impurity solver” for which several standard techniques are available such as (continuous-time) quantum Monte Carlo [(CT)QMC] [44,45], exact diagonalization [46,47], NRG (numerical renormalization group) [48,49], and others [50], each of which has both advantage and disadvantage. Another important issue is related to  $\hat{\Sigma}_{\text{dc}}(i\omega_n)$  for which many different recipes have been discussed in literature [1,2,37,51,52]. In the current study, we take so-called “fully localized limit” as suggested in Ref. [2].

Our main concern here is about the projection for defining the correlated subspace  $\{|\chi_{\alpha}\rangle\}$  in the line of previous discussion [36–38]. Note that different projection method can lead to the different self-energy. Several different ways to construct localized orbitals have been suggested. For example, maximally localized Wannier function (MLWF) method is widely used in combination with different type of codes [53–55]. One can also take LMTO (linearized muffin-tin orbitals) [56], NMTO ( $n$ th order muffin-tin orbitals) [53], or resort to the real space embedding method [31].

As an alternative possible choice, we pay a special attention to “projective Wannier function (PWF)” method which is a straightforward way to define correlated orbitals [19,57]. It has been adopted in some standard computation schemes including LMTO [20], APW [58–60], and PAW [19,57]. The main idea of PWF is to project the localized atomic-like orbitals  $\{|\tilde{\chi}_{\alpha}\rangle\}$  onto the low-energy Bloch states

$$|\chi_{\alpha}\rangle = \frac{1}{N} \sum_{k,n}^{\epsilon_{kn} \in W} |kn\rangle \langle kn| \tilde{\chi}_{\alpha},$$

followed by orthogonalization procedure [19]. Here,  $N = \|\sum_{k,n}^{\epsilon_{kn} \in W} |kn\rangle \langle kn| \tilde{\chi}_{\alpha}\|$  is the normalization factor and  $W$  energy window within which the hybridization function  $\Delta(i\omega_n)$

is defined. Thus the result depends not only on the energy window  $W$  but also on the choice of initial local orbitals  $\{|\tilde{\chi}_{\alpha}\rangle\}$ . While the ambiguity related to the  $W$  range can be removed, at least in principle by taking the large enough energy window [36], the choice of the  $|\tilde{\chi}_{\alpha}\rangle$  is not straightforward. The different initial choice can lead to the different final result [59].

A purpose of our current work is to construct the optimal  $|\tilde{\chi}_{\alpha}\rangle$  for the nonorthogonal local orbital basis method. As mentioned above, the result of DFT+DMFT can critically depend on the choice of  $|\tilde{\chi}_{\alpha}\rangle$ . Nonorthogonality can introduce an ambiguity in the estimation of key physical quantities such as the number of electrons in  $d$  orbitals  $N_d$ . This poses a highly nontrivial issue not only because the correlated orbitals often get significantly hybridized with ligands but also because the numerical orthogonalization process usually introduces the undesirable mixing between the two. Here we suggest NAOs [42] as a set of the local correlated orbitals  $|\tilde{\chi}_{\alpha}\rangle$  for DFT+DMFT calculation. As illustrated in Fig. 1, this process can be inserted as an intermediate step between DFT and DMFT to complete the self-consistent loop. While “natural orbital” has been adopted for the basis set to solve the impurity model [61], we emphasize that the use of  $|\chi_{\alpha}^{\text{NAOs}}\rangle$  as  $|\tilde{\chi}_{\alpha}\rangle$  has never been reported for the first-principles DFT+DMFT.

The use of NAO as a local projector has notable advantages. As will be discussed in the below, this choice can certainly give the more intuitive charge counting for the correlated orbitals. Further, the construction of NAOs is found to be numerically stable. In the case of MLWF, for example, achieving the convergence can be an issue when the bands are strongly entangled. As for muffin-tin orbitals or PAOs, basically the similar ambiguity can be manifested in terms of the choice of local orbital radius. In this sense, the use of NAO can be a ‘natural’ choice regardless of the DFT basis types.

## B. Natural atomic orbital as a projector

The numerical PAOs basis in our DFT code, OPENMX, is constructed in a controlled way and therefore its localization is well identified [62,63]. The nonorthogonality issue, on the other hand, needs to be dealt with care. One straightforward way is just to take  $|\tilde{\chi}_{\alpha}\rangle = |\phi^{\text{PAOs}}\rangle$  as correlated orbitals and to reconstruct the ligand orbitals to be orthogonal with respect to  $|\tilde{\chi}_{\alpha}\rangle$  through, e.g., Schmidt orthogonalization procedure. This choice corresponds to “full” local projector in the previous DFT+ $U$  implementation [64]. Not surprisingly, however, this procedure overestimates the electron occupation in the correlated orbitals as discussed in the below (see Sec. III). Another possible choice, namely, Löwdin symmetric orthogonalization, is not the desirable method either because it treats the important atomic set (the AO with large occupations) and the less important AO (the almost empty AO) on the equal footing.

Here we note that NAOs can be determined in a physically motivated way and suitable for local orbitals of the given materials [42]. Mathematically, NAOs are defined by the eigen-orbitals of any given local occupation matrix [65]. For a given occupation matrix  $N_{\alpha\beta}^{\text{PAOs}} = \langle c_{\alpha}^{\dagger} c_{\beta} \rangle$  NAOs are constructed through a three-step process. In the below, orbital

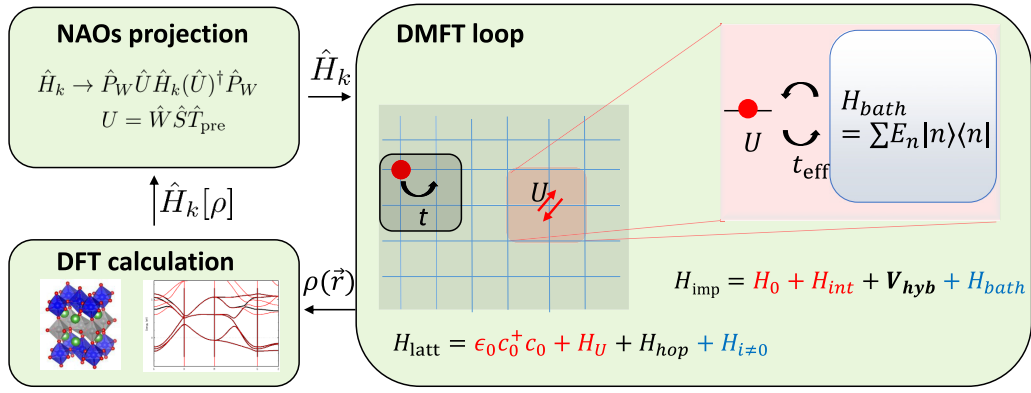


FIG. 1. A schematic illustration of our DFT+DMFT calculation by using NAO as local projector. Kohn-Sham DFT Hamiltonian is solved within LDA or GGA which provides the charge density and overlap matrix. With those, one can construct NAOs which then serve as correlated orbitals for DMFT impurity model. As in the conventional DFT+DMFT, Kohn-Sham Hamiltonian  $H_k$  obtained from LDA/GGA is regarded as noninteracting  $H_0$  for DMFT calculation. The computed Green's function  $G_{\text{imp}}$  and the self-energy  $\Sigma_{\text{imp}}$  complete the self-consistent loop by providing the updated charge density  $\rho(\vec{r})$  for DFT-LDA/GGA.

index  $\alpha \equiv (ilp)$  specifies the site index  $i$ , angular momentum quantum number  $l$ , and multiplicity number of radial basis function  $p$ . First, we construct the atom-centered local orbitals  $|\phi^{\text{pre}}\rangle$  called as “pre-NAOs” which are the eigenstates of the subblock  $(N^{i,l})_{pp}$  corresponding to the occupation matrix projected onto the atomic site  $i$  and the angular momentum  $l$  subshells. To preserve the invariance of the occupation with respect to the coordinate transformation, the symmetry averaging should be carried out over the  $(2l+1)$  diagonal blocks of  $N^{i,l}_{pp}$ . Since the pre-NAO transformation matrix  $\hat{T}_{\text{pre}}^{i,l}$  considers only the subblocks of the occupation matrix, pre-NAOs centered on different atoms are nonorthogonal to one another.

The second and third steps concern about the proper elimination of inter-atomic wave function overlaps. To obtain a stable result, we divide pre-NAOs into two subsets, namely, “minimal” and “Rydberg” set [42]. The minimal set is the atomic  $(n, l)$  subshells with finite formal occupancy whereas the Rydberg set consists of the remaining (formally unoccupied) orbitals. Then the Rydberg sets are Schmidt orthogonalized to the manifold spanned by minimal orbitals. We represent this orthogonalization by a matrix  $\hat{S}$ . This step is essential to avoid the over-counting problem in the occupancy-weighted symmetric orthogonalization (OWSO) process in the next step.

In the third step, we orthogonalize pre-NAOs orbitals by means of OWSO method in which the occupancy-weighted difference between orthogonalized basis and original pre-NAOs

$$\sum_{\alpha} N_{\alpha\alpha} \| |\chi_{\alpha}^{\text{NAOs}}\rangle - |\phi_{\alpha}^{\text{pre}}\rangle \|^2 \quad (3)$$

is minimized. Here,  $N$  is expressed within pre-NAOs basis. The transformation having this property is written as

$$|\chi_{\alpha}^{\text{NAOs}}\rangle = |\phi_{\beta}^{\text{PAOs}}\rangle W_{\beta\alpha}, \quad (4)$$

where  $\hat{W} = \tilde{N}(\tilde{N}O\tilde{N})^{-1/2}$  with the overlap matrix of pre-NAOs ( $O$ ), and the diagonal part of  $N$  ( $\tilde{N}$ ). The final form of transformation matrix from PAOs to NAOs can then be written as  $\hat{T}_N = \hat{W}\hat{S}\hat{T}_{\text{pre}}$ .

Natural orbital methods, including NAO and natural bond orbital, have been used typically to calculate atomic charge population [42,66]. Recently, natural orbitals have also been used to solve impurity problem of strongly correlated electron systems [67,68]. For example, natural orbitals can provide the adaptive basis set to reduce the dimension of Hilbert space [67]. In Ref. [68], model parameters for Anderson impurity problem have been obtained based on NAOs. In the current study, we used NAO as a basis or a projector for representing correlated subspace. We also demonstrate that the use of NAO can provide a way of reducing computation costs by separating the correlated orbitals into two subsets and adopting two different levels of solvers as will be discussed in the below.

### III. APPLICATION

#### A. Computation details

First-principles band calculations have been carried out based on DFT within LDA [69,70]. We used OPENMX code [43,62,63] for DFT calculation. Experimental lattice parameters have been used [71,72], and the  $k$ -point meshes of  $13 \times 13 \times 13$  and  $23 \times 23 \times 23$  adopted for SrVO<sub>3</sub> and NiO, respectively. Double valence and single polarization orbitals were used as a basis set for DFT. These numerical atomic basis orbitals (i.e., PAOs) were generated with cutoff radius of 10.0, 6.0, 6.0, and 5.0 a.u. for Sr V, Ni, and O atoms, respectively [62]. The DFT-LDA calculation results serve as the noninteracting Hamiltonian  $H_0$ , and the interaction Hamiltonian containing the density-density interaction is parameterized by  $U$  and  $J_H$  for on-site Coulomb repulsion and Hund interaction, respectively. The Hamiltonian is solved within the single-site DMFT by employing hybridization expansion CT-QMC algorithm [73,74]. For “impurity solver,” we used the software package as implemented in Refs. [75,76], and the results were double checked by using ALPS library [29]. Our DFT+DMFT interface code is available online [28]. The real frequency self-energy and spectral function are obtained from the matsubara Green's function and the self-energy by analytic continuation using maximum entropy method

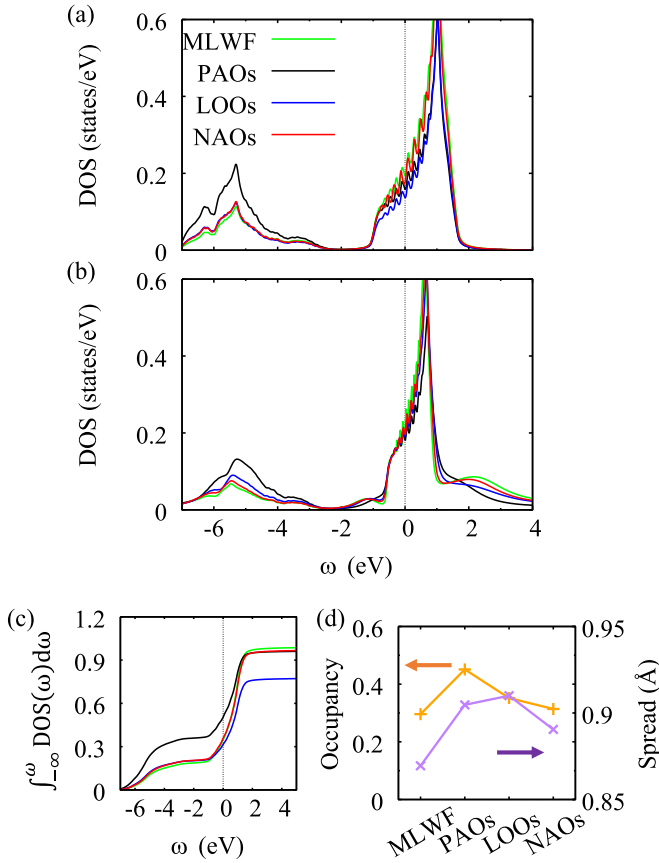


FIG. 2. (a) The calculated density of states projected onto the  $V-t_{2g}$ -like orbitals for  $\text{SrVO}_3$  with  $U = 0$  eV. The results from the different local orbitals, namely, MLWF (green), PAOs (black), LOOs (blue), and NAOs (red), are compared. (b) The calculated spectral function  $A(\omega)$  projected onto the local orbitals with  $U = 6$  eV and at inverse temperature  $\beta = 20$  eV $^{-1}$ . (c) The integrated density of states for different local orbitals. (d) The calculated occupancy of each  $t_{2g}$  orbitals within LDA+DMFT calculation (orange) and the spread of the orbitals as defined in the text (purple).

(MEM) [77,78]. For this process we used our recent method as reported in Ref. [79]. The large enough energy windows of  $W = [-10, 10]$  eV around  $E_F$  has been considered [36,71]. For comparison, we also present the results of MLWF as local projectors where the initial projections onto three atomic  $V-t_{2g}$  and nine O- $2p$  orbitals were used for  $\text{SrVO}_3$  [32,33].

### B. $\text{SrVO}_3$

$\text{SrVO}_3$  has been serving as a test bed for DFT+DMFT [59,80–83] and the related methods such as LDA+DCA [84] and GW+DMFT [85–89]. With cubic  $\text{SrVO}_3$  as our first example, we investigated the properties of NAO as a local projector. Figures 2(a) and 2(b) show the LDA ( $U = 0$  eV) and the LDA+DMFT density of states (DOS) projected onto the  $V-t_{2g}$ -like orbitals, respectively. Two main peaks are clearly identified; the  $O_p-V_d$  bonding complex locating at around  $[-7$  eV,  $-3$  eV], and the antibonding states across  $E_F$  which are mainly of  $V_d$  character. The results of four different projectors are presented in different colors,

namely, the green, black, blue, and red lines refer to the MLWF, PAO, LOO, and NAO result, respectively.

Not surprisingly, the degree of hybridization depends on the choice of projectors. For example, the direct use of PAOs notably overestimates  $d-p$  hybridization compared to the other projection methods. This feature is reflected in that the more states of the lower-lying bonding complex are assigned as  $V_d$  orbitals; see Figs. 2(a) and 2(b). Also, it naturally affects the electron number counting. With PAO projector,  $n_{e_g}^{\text{LDA}} = \sum_{n,k}^{\epsilon_{nk} < \epsilon_F} |\langle nk | \tilde{\chi}_{\alpha}^{\text{PAO}} |^2 = 0.55$  and  $n_{t_{2g}}^{\text{LDA}} = \sum_{n,k}^{\epsilon_{nk} < \epsilon_F} |\langle nk | \tilde{\chi}_{\beta}^{\text{PAO}} |^2 = 0.50$ , where  $\alpha \in e_g$  and  $\beta \in t_{2g}$ . Both values of  $n_{t_{2g}}^{\text{LDA}}$  and  $n_{e_g}^{\text{LDA}}$  are notably larger than those of NAOs;  $n_{e_g}^{\text{LDA}} = 0.29$  and  $n_{t_{2g}}^{\text{LDA}} = 0.35$ . The nominal values ( $t_{2g}^1$  configuration of  $V^{4+}$ ) are  $n_{e_g} = 0$  and  $n_{t_{2g}} = 1/6$ . Note that  $n_{t_{2g}}^{\text{LDA}} < n_{e_g}^{\text{LDA}}$  in PAO projection whereas  $n_{t_{2g}}^{\text{LDA}} > n_{e_g}^{\text{LDA}}$  in NAO.

The same feature can also be noted in the integrated DOS (IDOS) as presented in Fig. 2(c). The calculated IDOS at  $E_F$  clearly shows that the  $V_d$  occupation or its valency is markedly larger in the PAO estimation than in others. The calculated IDOS at  $E = E_F$  is 0.34, 0.50, 0.31, and 0.35 for MLWF, PAO, LOO, and NAO, respectively. The largest value of PAO projector reflects the greatest  $d-p$  hybridization while the value of NAO is smaller than that of PAO and comparable with MLWF. Another notable feature is that the IDOS calculated from LOOs does not reach to but remains far below 1.0 even up to  $\omega = +10$  eV;  $\simeq 0.78$ . On the other hand, the use of PAO and NAO projector satisfies the sum rule, yielding the IDOS  $\simeq 0.96$  and  $0.97$  (i.e., close to 1.0), respectively, as  $\omega$  becomes large.

This feature remains stable even when the number of basis orbitals (not the projector orbitals) changes. The calculation with the more basis orbitals of  $s2p2d2f1$  (i.e., double orbital sets for  $s$ ,  $p$ ,  $d$ , and single for  $f$  states), for example, gives  $n_{t_{2g}}^{\text{LDA}} = 0.31$  by using NAO projector. The calculated IDOS up to high energy remains as 0.97. On the other hand, the IDOS result of LOO, 0.72, shows the sizable dependence on the basis set choice due to the mixing between the correlated orbitals near  $E_F$  and the atomic orbitals in the higher energy. These features can certainly be useful for both practically and physically.

In order to see and compare the degree of spatial localization of correlated orbitals produced by different projectors, we computed the “spread function” [33] defined by  $\Omega = \sqrt{\langle \mathbf{r}^2 \rangle - \langle \mathbf{r} \rangle^2}$  where  $\langle \mathbf{r} \rangle = \int \mathbf{r} |\tilde{\chi}_{\alpha \in t_{2g}}(\mathbf{r})|^2 d\mathbf{r}$ . The results of the energy window  $W = [-10, 10]$  eV are presented in Fig. 2(d).

The calculated  $\Omega$  for NAOs is 0.891 Å which is slightly larger than that of MLWF (0.870 Å), and smaller than PAO (0.905 Å) and LOO (0.910 Å). Our analysis shows that the NAO projector produces a moderately localized spatial subspace of correlation.

The DFT+DMFT result of  $A(\omega) = -1/\pi \Im G_{\text{loc}}(\omega)$  is presented in Fig. 2(b). The calculations were performed with the inverse temperature  $\beta = 20$  eV $^{-1}$ ,  $U = 6.5$  eV, and  $J_H = 0.65$  eV [19]. The effect of correlation is clearly seen in the bandwidth renormalization and the upper Hubbard-like peak developed at around  $\omega = +2$  eV, both of which clearly show that the correlation effect is gradually reduced as the more

localized projector is adopted. The use of NAO gives the moderate degree of correlation in between MLWF and PAO. Focusing on the lower and upper Hubbard peak, identified at around  $\omega = -1$  and  $+2.5$  eV, respectively, they are more pronounced in the result of MLWF than PAO. Once again, the result of NAO is in the middle being consistent with the above analysis. A systematic trend of correlation strength depending on the local projectors is also observed in the calculated spectral weight of the bonding orbital complex. The calculated  $A(\omega)$  with PAO projector has the much greater weight in this region of energy reflecting the larger hybridization between  $V-t_{2g}$  and  $O-p$  states. This is attributed to the extended and nonorthogonal nature of PAO.

Figure 2(d) also shows the electron occupancy in  $V_{t_{2g}}$  orbitals,  $n_{t_{2g}}^{\text{DMFT}}$ , obtained from LDA+DMFT calculation with different local projectors. The NAO shows the comparable value with that of MLWF which is noticeably smaller than the other projection results. The use of more localized projector results in the smaller occupation which is consistent with the previous studies on covalency issue [36–38].

A straightforward and quantitative way to measure the correlation effect is to estimate the quasi-particle renormalization factor

$$Z \approx \left[ 1 - \frac{\Im \Sigma(i\omega_1)}{\omega_1} \right]^{-1}. \quad (5)$$

The calculated value by NAO projector is  $Z^{\text{NAO}} = 0.60$  which is comparable with that of MLWF ( $Z^{\text{MLWF}} = 0.58$ ). The result of PAO and LOO is  $Z^{\text{PAOs}} = 0.62$  and  $Z^{\text{Löwdin}} = 0.61$ , respectively. While these calculation results are in overall good agreement with the previous DFT+DMFT calculation of 0.61 [59] and ARPES (angle-resolved photoemission spectroscopy) of 0.56 [90], the degree of correlation effect is once again follow the same trend discussed above.

One big advantage of using our NAO projector is to reliably separate the correlated subspace into two parts. It enables us to use an elaborate technique only for the one part of correlated orbitals while, for another part, a computationally cheaper approximation can be utilized; or high-level approximation can be adopted for both parts, which are then embedded by the self-energy obtained from the cheaper approximation as shown in recent model studies [61,91,92]. In this scheme, natural orbitals were used as a basis set to represent the correlated subspace by taking only the orbitals whose occupations are close to 1.0.

We apply this type of capability to the first-principles DFT+DMFT framework. In order to see its effect, we extend the correlated subspace from three  $t_{2g}$  orbitals to the  $d$  complex (i.e., both  $t_{2g} + e_g$ ). The former is certainly more relevant to the correlation effect and basically determines the most of electronic properties while the latter is less important. Therefore we adopted CTQMC solver for  $t_{2g}$  orbitals and the second-order perturbation theory (2PT) for  $e_g$ , which significantly reduces the computation cost. For more details of our 2PT method, see Appendix.

The calculation result of spectral function is presented as a blue line in Fig. 3. The red line in Fig. 3 represents the CTQMC-only result; namely, all of five  $V-d$  orbitals are solved with CTQMC. In spite of much less computation cost

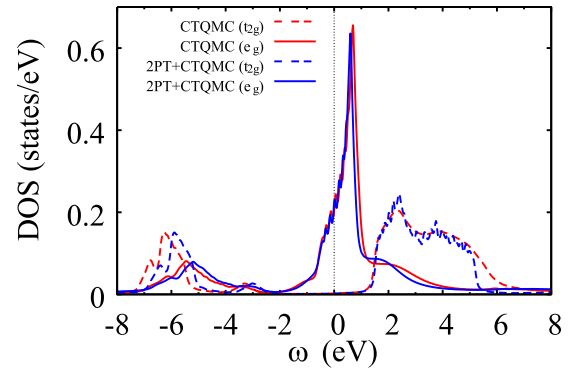


FIG. 3. The calculated spectral function for SrVO<sub>3</sub> projected onto the  $V-e_g$  (dashed line) and  $t_{2g}$  (solid line) orbitals. The result presented in red color is obtained with CTQMC solver for five  $V-d$  orbitals. The blue colored lines present the result obtained by CTQMC solver for three  $V-t_{2g}$  orbitals whose self-energy is then embedded into the second-order perturbation theory (2PT) solution.

(i.e., five- versus three-orbital impurity problem for CTQMC), the hybrid solver of 2PT+CTQMC gives a reasonable agreement with the CTQMC-only result especially for the near- $E_F$  region. For example, Hubbard bands and the  $d-p$  hybridization part are well reproduced. Simultaneously, some deviations are also clearly noticed. For example, the intensity of the Hubbard bands are reduced in 2PT+CTQMC calculation. This reduced correlation in  $t_{2g}$  manifolds is attributed to the inability of 2PT to accurately describe the screening effect [93,94]. As expected, the difference between the two computation results is more pronounced in high energy  $e_g$  spectra.

### C. NiO

As the second example, we chose a classical charge-transfer insulator NiO. Due to the sizable hybridization between Ni- $d$  and O- $p$ , the electronic property depends on the choice of local correlated orbital projector. Note that the projector affects both Hubbard  $U$  and charge-transfer energy  $\Delta$  in this type of materials [37,38,95]. The inverse temperature of  $\beta = 10$  eV<sup>-1</sup> (corresponding to 1160.45 K higher than Neel temperature  $T_N = 525$  K [96,97]) and the interaction parameters of  $U = 8$  eV and  $J_H = 1$  eV were used following the previous studies [1,51,98]. Figure 4 shows the electronic structures which were calculated by two different projectors; (a) PAO and (b) NAO. As expected, LDA ( $U = 0$ ; black solid line) gives the unphysical metallic solution while the experimental gap is  $\sim 4.3$  eV [99].

The DFT+DMFT spectral function  $A(\mathbf{k}, \omega)$  calculated with PAO projector is presented as a false-color band in Fig. 4(a). Interestingly the system remains metallic in a sharp contrast to the previous calculations of DFT+ $U$  [1,64] and DFT+DMFT [51,98]. This result demonstrates the fact that the effect of correlations depend on the choice of local projector. Note that the Ni- $e_g$  energy level  $\epsilon^{e_g} = \langle \hat{H} \rangle_{\chi^{\text{PAOs}}} = -7.58$  eV is significantly lower than that of NAO (see below) which results in the large number of Ni- $d$  electrons,  $N_d = 8.72$ . In combination with the conventional FLL double counting, it leads to a significant change of chemical potential.

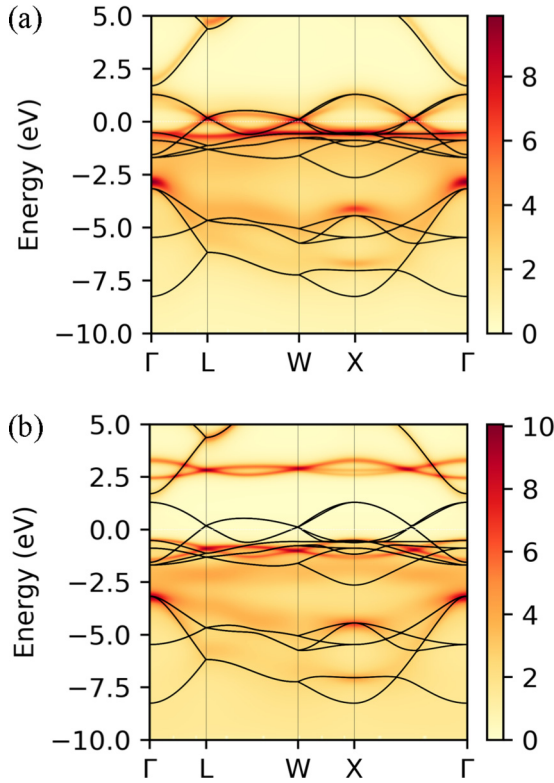


FIG. 4. The calculated band dispersion of NiO. DFT+DMFT result (color map) is compared with that of LDA (black solid lines). Two different projection methods are adopted for DFT+DMFT calculation; (a) PAOs and (b) NAOs.

This effect is clearly noticed, for example, in the bands at around  $\pm \sim 2.5$  eV being deviated from LDA bands.

The result of NAO projector is presented in Fig. 4(b) (false color plot) in comparison with LDA (black line). A well developed band gap is clearly identified. The on-site energy is significantly increased compared to PAO result,  $\epsilon_d^{eg} = -7.21$  eV, and therefore the charge transfer energy is increased. The  $d$  orbital occupancy is also reduced  $N_d = 8.21$ . It is found that the electronic structure is overall quite consistent with previous theoretical studies [51,64,98].

#### IV. SUMMARY

We introduce NAO as a local projector to define the correlated subspace in DFT+DMFT procedure. Our implementation is based on the systematic construction of projector from the original nonorthogonal PAO basis set. We apply this method to a correlated metal SrVO<sub>3</sub> and insulator NiO. From the comparison with other projector methods, we found that NAO not just serves as another possible choice, but it also has some advantage particularly in the charge counting. First, it provides a reliable electron number  $N_d$  for the correlated orbitals and does not require any additional convergence or minimization procedure. No arbitrary numerical parameter needs to be introduced such as cutoff or muffin-tin radius, and the application to the entangled band structure is also straightforward. Finally, we emphasize that the use of NAO projector provides a viable way to separate correlated subspace into two parts; one for which the elaborate technique can be used for

describing correlations, and for another part one can resort to a computationally cheaper approximation.

#### ACKNOWLEDGMENTS

We thank Hongkee Yoon for useful comment and discussion. This work was supported by the Basic Science Research Program through the National Research Foundation of Korea (NRF) funded by the Ministry of Education (2018R1A2B2005204) and Creative Materials Discovery Program through the NRF funded by Ministry of Science and ICT (2018M3D1A1059001).

#### APPENDIX: DETAILS OF THE SECOND-ORDER PERTURBATION APPROACH

Our DFT+DMFT iteration procedure with 2PT+CTQMC solver is summarized as follows.

(1) We start with the initial guess for self-energy  $\Delta\Sigma(i\omega_n) = \Sigma_{\text{weak}} + \Sigma_{\text{strong}} - \Sigma_{\text{DC}}^{\text{DFT}} = 0$ . The local Green's function of a given material (or lattice problem) is

$$G_{\text{loc}}(i\omega_n) = \frac{1}{N_k} \sum_k [i\omega_n - H_k + \mu - \Delta\Sigma(i\omega_n)]^{-1}, \quad (\text{A1})$$

where  $H_k$  is the Kohn-Sham Hamiltonian and the chemical potential  $\mu$  is adjusted to obtain the correct number of electrons.

(2) Calculate Weiss mean-field  $\mathcal{G}^{-1} = G_{\text{loc}}^{-1} + \Sigma_{\text{imp}}$ . Equivalently one can calculate the impurity energy level and the hybridization function from  $H_{\text{imp}} = H_{\text{loc}} - \Sigma_{\text{DC}}^{\text{DFT}}$  and  $\Delta = i\omega_n - H_{\text{loc}} + \mu - \Delta\Sigma - G_{\text{loc}}^{-1}$ , respectively.

(3) Now we solve the impurity problem with an approximate way. Here we adopted the second-order perturbation theory:

$$\Sigma^{(2)}(i\omega_n) = \Sigma^{\text{HF}}[G_{\text{loc}}] + \Sigma'^{(2)}[G_{\text{HF}}](i\omega_n), \quad (\text{A2})$$

where  $\Sigma^{\text{HF}}$  is the Hartree-Fock contribution and

$$\begin{aligned} \Sigma'^{(2)}[G](i\omega_n) = & (-G_{kl}(\tau)G_{mn}(\tau)G_{pq}(-\tau) \\ & + G_{kn}(\tau)G_{ml}(\tau)G_{pq}(-\tau))U_{iqmk}U_{lnpj}. \end{aligned} \quad (\text{A3})$$

Here the summation over the repeated indices is assumed and  $U_{ijkl} = \langle ij|U|kl \rangle$ .

(4) Calculate the double counting term,  $\Sigma_{\text{DC}}^{(2)} = \Sigma^{\text{HF}}[\hat{P}_c G_{\text{loc}}] + \Sigma'^{(2)}[\hat{P}_c G_{\text{HF}}](i\omega_n)$ . Here  $\hat{P}_c$  is the projector onto the strongly correlated orbitals, namely,  $t_{2g}$  orbitals for SrVO<sub>3</sub>. Then we have  $\Sigma_{\text{weak}}(i\omega_n) = \Sigma^{(2)}(i\omega_n) - \Sigma_{\text{DC}}^{(2)}(i\omega_n)$ .

(5) CTQMC impurity solver is adopted to obtain the impurity self-energy  $\Sigma_{\text{strong}}$  describing the correlated subspace  $c$ . Again, we construct the impurity problem from the Weiss field  $\mathcal{G}_{\text{strong}}^{-1} = (P_c G_{\text{loc}})^{-1} + \Sigma_{\text{strong}}$ . Alternatively, we can define the impurity site energy  $H_{\text{imp}}^{\text{strong}} = H_{\text{loc}} + \Sigma_{\text{weak}}(\infty) - \Sigma_{\text{DC}}^{\text{DFT}}$  and the hybridization  $\Delta_{\text{strong}} = i\omega_n - H_{\text{imp}}^{\text{strong}} + \mu - \Sigma_{\text{strong}} - (P_c G_{\text{loc}})^{-1} \approx i\omega_n - H_{\text{loc}} + \mu - P_c(\Delta\Sigma) + \Sigma'_{\text{weak}} - (P_c G_{\text{loc}})^{-1}$ .

(6) Update  $\Delta\Sigma(i\omega_n) = \Sigma_{\text{weak}} + \Sigma_{\text{strong}} - \Sigma_{\text{DC}}^{\text{DFT}}$  and go back to step 2.

- [1] V. I. Anisimov, J. Zaanen, and O. K. Andersen, Band theory and Mott insulators: Hubbard U instead of Stoner I, *Phys. Rev. B* **44**, 943 (1991).
- [2] V. I. Anisimov, I. V. Solovyev, M. A. Korotin, M. T. Czyżyk, and G. A. Sawatzky, Density-functional theory and NiO photoemission spectra, *Phys. Rev. B* **48**, 16929 (1993).
- [3] K. M. Ho, J. Schmalian, and C. Z. Wang, Gutzwiller density functional theory for correlated electron systems, *Phys. Rev. B* **77**, 073101 (2008).
- [4] M. C. Gutzwiller, Correlation of Electrons in a Narrow  $s$  Band, *Phys. Rev.* **137**, A1726 (1965).
- [5] X. Y. Deng, L. Wang, X. Dai, and Z. Fang, Local density approximation combined with Gutzwiller method for correlated electron systems: Formalism and applications, *Phys. Rev. B* **79**, 075114 (2009).
- [6] N. Lanatà, Y. Yao, C.-Z. Wang, K.-M. Ho, and G. Kotliar, Phase Diagram and Electronic Structure of Praseodymium and Plutonium, *Phys. Rev. X* **5**, 011008 (2015).
- [7] M. van Schilfhaarde, T. Kotani, and S. Faleev, Quasiparticle Self-Consistent  $GW$  Theory, *Phys. Rev. Lett.* **96**, 226402 (2006).
- [8] T. Kotani, M. van Schilfhaarde, and S. V. Faleev, Quasiparticle self-consistent  $GW$  method: A basis for the independent-particle approximation, *Phys. Rev. B* **76**, 165106 (2007).
- [9] S. V. Faleev, M. van Schilfhaarde, and T. Kotani, All-Electron Self-Consistent  $GW$  Approximation: Application to Si, MnO, and NiO, *Phys. Rev. Lett.* **93**, 126406 (2004).
- [10] S. W. Jang, T. Kotani, H. Kino, K. Kuroki, and M. J. Han, Quasiparticle self-consistent  $GW$  study of cuprates: Electronic structure, model parameters, and the two-band theory for  $T_c$ , *Sci. Rep.* **5**, 12050 (2015).
- [11] S. Ryee, S. W. Jang, H. Kino, T. Kotani, and M. J. Han, Quasiparticle self-consistent  $GW$  calculation of  $\text{Sr}_2\text{RuO}_4$  and  $\text{SrRuO}_3$ , *Phys. Rev. B* **93**, 075125 (2016).
- [12] A. Georges and G. Kotliar, Hubbard model in infinite dimensions, *Phys. Rev. B* **45**, 6479 (1992).
- [13] W. Metzner and D. Vollhardt, Correlated Lattice Fermions in  $d = \infty$  Dimensions, *Phys. Rev. Lett.* **62**, 324 (1989).
- [14] X. Y. Zhang, M. J. Rozenberg, and G. Kotliar, Mott Transition in the  $d = \infty$  Hubbard Model at Zero Temperature, *Phys. Rev. Lett.* **70**, 1666 (1993).
- [15] V. I. Anisimov, A. I. Poteryaev, M. A. Korotin, A. O. Anokhin, and G. Kotliar, First-principles calculations of the electronic structure and spectra of strongly correlated systems: Dynamical mean-field theory, *J. Phys. Condens. Matter* **9**, 7359 (1997).
- [16] A. I. Lichtenstein and M. I. Katsnelson, *Ab initio* calculations of quasiparticle band structure in correlated systems: LDA++ approach, *Phys. Rev. B* **57**, 6884 (1998).
- [17] G. Kotliar, S. Y. Savrasov, K. Haule, V. S. Oudovenko, O. Parcollet, and C. A. Marianetti, Electronic structure calculations with dynamical mean-field theory, *Rev. Mod. Phys.* **78**, 865 (2006).
- [18] A. Georges, G. Kotliar, W. Krauth, and M. J. Rozenberg, Dynamical mean-field theory of strongly correlated fermion systems and the limit of infinite dimensions, *Rev. Mod. Phys.* **68**, 13 (1996).
- [19] B. Amadon, F. Lechermann, A. Georges, F. Jollet, T. O. Wehling, and A. I. Lichtenstein, Plane-wave based electronic structure calculations for correlated materials using dynamical mean-field theory and projected local orbitals, *Phys. Rev. B* **77**, 205112 (2008).
- [20] V. I. Anisimov, D. E. Kondakov, A. V. Kozhevnikov, I. A. Nekrasov, Z. V. Pchelkina, J. W. Allen, S. K. Mo, H. D. Kim, P. Metcalf, S. Suga, A. Sekiyama, G. Keller, I. Leonov, X. Ren, and D. Vollhardt, Full orbital calculation scheme for materials with strongly correlated electrons, *Phys. Rev. B* **71**, 125119 (2005).
- [21] S. Y. Savrasov, G. Kotliar, and E. Abrahams, Correlated electrons in  $\delta$ -plutonium within a dynamical mean-field picture, *Nature (London)* **410**, 793 (2001).
- [22] K. Held, A. K. McMahan, and R. T. Scalettar, Cerium Volume Collapse: Results from the Merger of Dynamical Mean-Field Theory and Local Density Approximation, *Phys. Rev. Lett.* **87**, 276404 (2001).
- [23] K. Held, G. Keller, V. Eyert, D. Vollhardt, and V. I. Anisimov, Mott-Hubbard Metal-Insulator Transition in Paramagnetic  $\text{V}_2\text{O}_3$ : An LDA + DMFT(QMC) Study, *Phys. Rev. Lett.* **86**, 5345 (2001).
- [24] H. Park, K. Haule, and G. Kotliar, Cluster Dynamical Mean Field Theory of the Mott Transition, *Phys. Rev. Lett.* **101**, 186403 (2008).
- [25] L. de' Medici, J. Mravlje, and A. Georges, Janus-Faced Influence of Hund's Rule Coupling in Strongly Correlated Materials, *Phys. Rev. Lett.* **107**, 256401 (2011).
- [26] P. R. C. Kent and G. Kotliar, Toward a predictive theory of correlated materials, *Science* **361**, 348 (2018).
- [27] S. Choi, P. Semon, B. Kang, A. Kutepov, and G. Kotliar, ComDMFT: A massively parallel computer package for the electronic structure of correlated-electron systems, *Comput. Phys. Commun.* **244**, 277 (2019).
- [28] DMFTpack, <https://kaist-elst.github.io/DMFTpack/>.
- [29] F. Alet, P. Dayal, A. Grzesik, A. Honecker, M. K. Orner, A. L. Auhl, S. R. Manmana, I. P. McCulloch, F. Michel, R. M. Noack, G. Schmid, U. Schollwöck, F. Stöckli, S. Todo, S. Trebst, M. Troyer, P. Werner, and S. Wessel, The ALPS project treasury 2.0: Open source software for strongly correlated systems, *J. Phys. Soc. Jpn.* **74**, 30 (2005).
- [30] O. Parcollet, M. Ferrero, T. Ayril, H. Hafermann, I. Krivenko, L. Messio, and P. Seth, TRIQS: A toolbox for research on interacting quantum systems, *Comput. Phys. Commun.* **196**, 398 (2015).
- [31] K. Haule, C.-H. Yee, and K. Kim, Dynamical mean-field theory within the full-potential methods: Electronic structure of  $\text{CeIrIn}_5$ ,  $\text{CeCoIn}_5$ , and  $\text{CeRhIn}_5$ , *Phys. Rev. B* **81**, 195107 (2010).
- [32] I. Souza, N. Marzari, and D. Vanderbilt, Maximally-localized Wannier functions for entangled energy bands, *Phys. Rev. B* **65**, 035109 (2001).
- [33] N. Marzari and D. Vanderbilt, Maximally localized generalized Wannier functions for composite energy bands, *Phys. Rev. B* **56**, 12847 (1997).
- [34] O. K. Andersen and T. Saha-Dasgupta, Muffin-tin orbitals of arbitrary order, *Phys. Rev. B* **62**, R16219 (2000).
- [35] E. Pavarini, S. Biermann, A. Poteryaev, A. I. Lichtenstein, A. Georges, and O. K. Andersen, Mott Transition and Suppression of Orbital Fluctuations in Orthorhombic  $3d^1$  Perovskites, *Phys. Rev. Lett.* **92**, 176403 (2004).

- [36] K. Haule, T. Birol, and G. Kotliar, Covalency in transition-metal oxides within all-electron dynamical mean-field theory, *Phys. Rev. B* **90**, 075136 (2014).
- [37] X. Wang, M. J. Han, L. de' Medici, H. Park, C. A. Marianetti, and A. J. Millis, Covalency, double-counting, and the metal-insulator phase diagram in transition metal oxides, *Phys. Rev. B* **86**, 195136 (2012).
- [38] H. T. Dang, A. J. Millis, and C. A. Marianetti, Covalency and the metal-insulator transition in titanate and vanadate perovskites, *Phys. Rev. B* **89**, 161113(R) (2014).
- [39] R. S. Mulliken, Electronic Population Analysis on LCAO-MO Molecular Wave Functions. I, *J. Chem. Phys.* **23**, 1833 (1955).
- [40] R. S. Mulliken, Electronic population analysis on LCAO-MO molecular wave functions. II. Overlap populations, bond orders, and covalent bond energies, *J. Chem. Phys.* **23**, 1841 (1955).
- [41] P. O. Löwdin, On the non-orthogonality problem connected with the use of atomic wave functions in the theory of molecules and crystals, *J. Chem. Phys.* **18**, 365 (1950).
- [42] A. E. Reed, R. B. Weinstock, and F. Weinhold, Natural population analysis, *J. Chem. Phys.* **83**, 735 (1985).
- [43] OPENMX, <http://www.openmx-square.org>.
- [44] P. Werner, A. Comanac, L. de' Medici, M. Troyer, and A. J. Millis, Continuous-Time Solver for Quantum Impurity Models, *Phys. Rev. Lett.* **97**, 076405 (2006).
- [45] P. Werner and A. J. Millis, Hybridization expansion impurity solver: General formulation and application to Kondo lattice and two-orbital models, *Phys. Rev. B* **74**, 155107 (2006).
- [46] E. Koch, G. Sangiovanni, and O. Gunnarsson, Sum rules and bath parametrization for quantum cluster theories, *Phys. Rev. B* **78**, 115102 (2008).
- [47] M. Caffarel and W. Krauth, Exact Diagonalization Approach to Correlated Fermions in Infinite Dimensions: Mott Transition and Superconductivity, *Phys. Rev. Lett.* **72**, 1545 (1994).
- [48] K. G. Wilson, The renormalization group: Critical phenomena and the Kondo problem, *Rev. Mod. Phys.* **47**, 773 (1975).
- [49] R. Bulla, T. A. Costi, and T. Pruschke, Numerical renormalization group method for quantum impurity systems, *Rev. Mod. Phys.* **80**, 395 (2008).
- [50] D. Bauernfeind, M. Zingl, R. Triebl, M. Aichhorn, and H. G. Evertz, Fork tensor-product states: Efficient multiorbital real-time DMFT solver, *Phys. Rev. X* **7**, 031013 (2017).
- [51] M. Karolak, G. Ulm, T. Wehling, V. Mazurenko, A. Poteryaev, and A. Lichtenstein, Double counting in LDA+DMFT—The example of NiO, *J. Electron Spectrosc. Relat. Phenom.* **181**, 11 (2010).
- [52] K. Haule, Exact Double Counting in Combining the Dynamical Mean Field Theory and the Density Functional Theory, *Phys. Rev. Lett.* **115**, 196403 (2015).
- [53] F. Lechermann, A. Georges, A. Poteryaev, S. Biermann, M. Posternak, A. Yamasaki, and O. K. Andersen, Dynamical mean-field theory using Wannier functions: A flexible route to electronic structure calculations of strongly correlated materials, *Phys. Rev. B* **74**, 125120 (2006).
- [54] S. Bhandary, E. Assmann, M. Aichhorn, and K. Held, Charge self-consistency in density functional theory combined with dynamical mean field theory:  $k$ -space reoccupation and orbital order, *Phys. Rev. B* **94**, 155131 (2016).
- [55] DCore, <https://issp-center-dev.github.io/DCore/>.
- [56] L. V. Pourovskii, B. Amadon, S. Biermann, and A. Georges, Self-consistency over the charge density in dynamical mean-field theory: A linear muffin-tin implementation and some physical implications, *Phys. Rev. B* **76**, 235101 (2007).
- [57] B. A. Amadon, A self-consistent DFT+DMFT scheme in the projector augmented wave method: Applications to cerium,  $\text{Ce}_2\text{O}_3$  and  $\text{Pu}_2\text{O}_3$  with the Hubbard I solver and comparison to DFT+U, *J. Phys. Condens. Matter* **24**, 075604 (2012).
- [58] M. Aichhorn, L. Pourovskii, V. Vildosola, M. Ferrero, O. Parcollet, T. Miyake, A. Georges, and S. Biermann, Dynamical mean-field theory within an augmented plane-wave framework: Assessing electronic correlations in the iron pnictide  $\text{LaFeAsO}$ , *Phys. Rev. B* **80**, 085101 (2009).
- [59] M. Karolak, T. O. Wehling, F. Lechermann, and A. I. Lichtenstein, General DFT++ method implemented with projector augmented waves: Electronic structure of  $\text{SrVO}_3$  and the Mott transition in  $\text{Ca}_{2-x}\text{Sr}_x\text{RuO}_4$ , *J. Phys. Condens. Matter* **23**, 085601 (2011).
- [60] M. Schüler, O. E. Peil, G. J. Kraberger, R. Pordzik, M. Marsman, G. Kresse, T. O. Wehling, and M. Aichhorn, Charge self-consistent many-body corrections using optimized projected localized orbitals, *J. Phys.: Condens. Matter* **30**, 475901 (2018).
- [61] A. A. Kananenka, E. Gull, and D. Zgid, Systematically improvable multiscale solver for correlated electron systems, *Phys. Rev. B* **91**, 121111(R) (2015).
- [62] T. Ozaki and H. Kino, Numerical atomic basis orbitals from H to Kr, *Phys. Rev. B* **69**, 195113 (2004).
- [63] T. Ozaki, Variationally optimized atomic orbitals for large-scale electronic structures, *Phys. Rev. B* **67**, 155108 (2003).
- [64] M. J. Han, T. Ozaki, and J. Yu,  $O(N)$  LDA+ $U$  electronic structure calculation method based on the nonorthogonal pseudoatomic orbital basis, *Phys. Rev. B* **73**, 045110 (2006).
- [65] P.-O. Löwdin, Quantum theory of many-particle systems. I. Physical interpretations by means of density matrices, natural spin-orbitals, and convergence problems in the method of configurational interaction, *Phys. Rev.* **97**, 1474 (1955).
- [66] A. E. Reed, L. A. Curtiss, and F. Weinhold, Intermolecular interactions from a natural bond orbital, donor-acceptor viewpoint, *Chem. Rev.* **88**, 899 (1988).
- [67] A. Go and A. J. Millis, Adaptively truncated Hilbert space based impurity solver for dynamical mean-field theory, *Phys. Rev. B* **96**, 085139 (2017).
- [68] S. Mayda, Z. Kandemir, and N. Bulut, Electronic Structure of Cyanocobalamin: DFT+QMC Study, *J. Supercond. Nov. Magn.* **30**, 3301 (2017).
- [69] J. P. Perdew and A. Zunger, Self-interaction correction to density-functional approximations for many-electron systems, *Phys. Rev. B* **23**, 5048 (1981).
- [70] D. M. Ceperley and B. J. Alder, Ground State of the Electron Gas by a Stochastic Method, *Phys. Rev. Lett.* **45**, 566 (1980).
- [71] M. J. Rey, P. Dehault, J. C. Joubert, B. Lambert-Andron, M. Cyrot, and F. Cyrot-Lackmann, Preparation and structure of the compounds  $\text{SrVO}_3$  and  $\text{Sr}_2\text{VO}_4$ , *J. Solid State Chem.* **86**, 101 (1990).
- [72] R. Furstenuau, G. McDougall, and M. Langell, Initial stages of hydrogen reduction of  $\text{NiO}(100)$ , *Surf. Sci.* **150**, 55 (1985).
- [73] E. Gull, A. J. Millis, A. I. Lichtenstein, A. N. Rubtsov, M. Troyer, and P. Werner, Continuous-time Monte Carlo methods for quantum impurity models, *Rev. Mod. Phys.* **83**, 349 (2011).

- [74] E. Gull, P. Werner, S. Fuchs, B. Surer, T. Pruschke, and M. Troyer, Continuous-time quantum Monte Carlo impurity solvers, *Comput. Phys. Commun.* **182**, 1078 (2011).
- [75] K. Haule, Quantum Monte Carlo impurity solver for cluster dynamical mean-field theory and electronic structure calculations with adjustable cluster base, *Phys. Rev. B* **75**, 155113 (2007).
- [76] <http://hauleweb.rutgers.edu/tutorials/Tutorial0.html>.
- [77] M. Jarrell and J. E. Gubernatis, Bayesian inference and the analytic continuation of imaginary-time quantum Monte Carlo data, *Phys. Rep.* **269**, 133 (1996).
- [78] O. Gunnarsson, M. W. Haverkort, and G. Sangiovanni, Analytical continuation of imaginary axis data using maximum entropy, *Phys. Rev. B* **81**, 155107 (2010).
- [79] J.-H. Sim and M. J. Han, Maximum quantum entropy method, *Phys. Rev. B* **98**, 205102 (2018).
- [80] I. A. Nekrasov, G. Keller, D. E. Kondakov, A. V. Kozhevnikov, T. Pruschke, K. Held, D. Vollhardt, and V. I. Anisimov, Comparative study of correlation effects in  $\text{CaVO}_3$  and  $\text{SrVO}_3$ , *Phys. Rev. B* **72**, 155106 (2005).
- [81] I. A. Nekrasov, K. Held, G. Keller, D. E. Kondakov, T. Pruschke, M. Kollar, O. K. Andersen, V. I. Anisimov, and D. Vollhardt, Momentum-resolved spectral functions of  $\text{SrVO}_3$  calculated by LDA+DMFT, *Phys. Rev. B* **73**, 155112 (2006).
- [82] A. Sekiyama, H. Fujiwara, S. Imada, S. Suga, H. Eisaki, S. I. Uchida, K. Takegahara, H. Harima, Y. Saitoh, I. A. Nekrasov, G. Keller, D. E. Kondakov, A. V. Kozhevnikov, T. Pruschke, K. Held, D. Vollhardt, and V. I. Anisimov, Mutual Experimental and Theoretical Validation of Bulk Photoemission Spectra of  $\text{Sr}_{1-x}\text{Ca}_x\text{VO}_3$ , *Phys. Rev. Lett.* **93**, 156402 (2004).
- [83] Y. Nomura, M. Kaltak, K. Nakamura, C. Taranto, S. Sakai, A. Toschi, R. Arita, K. Held, G. Kresse, and M. Imada, Effective on-site interaction for dynamical mean-field theory, *Phys. Rev. B* **86**, 085117 (2012).
- [84] H. Lee, K. Foyevtsova, J. Ferber, M. Aichhorn, H. O. Jeschke, and R. Valentí, Dynamical cluster approximation within an augmented plane wave framework: Spectral properties of  $\text{SrVO}_3$ , *Phys. Rev. B* **85**, 165103 (2012).
- [85] C. Taranto, M. Kaltak, N. Parragh, G. Sangiovanni, G. Kresse, A. Toschi, and K. Held, Comparing quasiparticle GW+DMFT and LDA+DMFT for the test bed material  $\text{SrVO}_3$ , *Phys. Rev. B* **88**, 165119 (2013).
- [86] M. Casula, A. Rubtsov, and S. Biermann, Dynamical screening effects in correlated materials: Plasmon satellites and spectral weight transfers from a Green's function ansatz to extended dynamical mean field theory, *Phys. Rev. B* **85**, 035115 (2012).
- [87] J. M. Tomczak, M. Casula, T. Miyake, and S. Biermann, Asymmetry in band widening and quasiparticle lifetimes in  $\text{SrVO}_3$ : Competition between screened exchange and local correlations from combined G W and dynamical mean-field theory GW + DMFT, *Phys. Rev. B* **90**, 165138 (2014).
- [88] J. M. Tomczak, M. Casula, T. Miyake, F. Aryasetiawan, and S. Biermann, Combined GW and dynamical mean-field theory: Dynamical screening effects in transition metal oxides, *Europhys. Lett.* **100**, 67001 (2012).
- [89] S. Choi, A. Kutepov, K. Haule, M. van Schilfhaarde, and G. Kotliar, First-principles treatment of Mott insulators: Linearized QSGW+DMFT approach, *Npj Quantum Materials* **1**, 16001 (2016).
- [90] T. Yoshida, K. Tanaka, H. Yagi, A. Ino, H. Eisaki, A. Fujimori, and Z.-X. Shen, Direct Observation of the Mass Renormalization in  $\text{SrVO}_3$  by Angle Resolved Photoemission Spectroscopy, *Phys. Rev. Lett.* **95**, 146404 (2005).
- [91] T. Nguyen Lan, A. A. Kananenka, and D. Zgid, Rigorous Ab Initio Quantum Embedding for Quantum Chemistry Using Green's Function Theory: Screened Interaction, Nonlocal Self-Energy Relaxation, Orbital Basis, and Chemical Accuracy, *J. Chem. Theory Comput.* **12**, 4856 (2016).
- [92] T. N. Lan, A. Shee, J. Li, E. Gull, and D. Zgid, Testing self-energy embedding theory in combination with GW, *Phys. Rev. B* **96**, 155106 (2017).
- [93] J. Gukelberger, L. Huang, and P. Werner, On the dangers of partial diagrammatic summations: Benchmarks for the two-dimensional Hubbard model in the weak-coupling regime, *Phys. Rev. B* **91**, 235114 (2015).
- [94] C. Honerkamp, H. Shinaoka, F. F. Assaad, and P. Werner, Limitations of constrained random phase approximation downfolding, *Phys. Rev. B* **98**, 235151 (2018).
- [95] J. Zaanen, G. A. Sawatzky, and J. W. Allen, Band Gaps and Electronic Structure of Transition-Metal Compounds, *Phys. Rev. Lett.* **55**, 418 (1985).
- [96] G. Srinivasan and M. S. Seehra, Nature of magnetic transitions in  $\text{MnO}$ ,  $\text{Fe}_2\text{O}$ ,  $\text{CoO}$ , and  $\text{NiO}$ , *Phys. Rev. B* **28**, 6542 (1983).
- [97] W. L. Roth, Multispin axis structures for antiferromagnets, *Phys. Rev.* **111**, 772 (1958).
- [98] J. Kuneš, V. I. Anisimov, A. V. Lukoyanov, and D. Vollhardt, Local correlations and hole doping in  $\text{NiO}$ : A dynamical mean-field study, *Phys. Rev. B* **75**, 165115 (2007).
- [99] S. Hüfner, J. Osterwalder, T. Riesterer, and F. Hulliger, Photoemission and inverse photoemission spectroscopy of  $\text{NiO}$ , *Solid State Commun.* **52**, 793 (1984).